Journal of Materials Chemistry A

Accepted Manuscript

ROYAL SOCIETY OF CHEMISTRY

www.rsc.org/materialsA

Cite this: DOI: 10.1039/c0xx00000x

www.rsc.org/xxxxxx

ARTICLE TYPE

Facile synthesis of mesoporous Co_3O_4/CeO_2 hybrid nanowire arrays for high performance supercapacitors

Jiewu Cui [a,b], Xinyi Zhang [c], Liang Tong [b], Jinbao Luo [a], Yan Wang [a,b], Yong Zhang [a,b], Kui Xie [a,b] and Yucheng Wu [*a,b]

Received (in XXX, XXX) Xth XXXXXXXXX 20XX, Accepted Xth XXXXXXXXX 20XX
DOI: 10.1039/b000000x

The development of porous yet densely packed nanomaterials with high ion-accessible surface area and long cycling life is critical to the realization of high-density electrochemical capacitive energy storage. In this paper, we report a facile hydrothermal method to fabricate Co_3O_4/CeO_2 hybrid nanowire arrays (NWAs). Supercapacitors based on the as-prepared mesoporous Co_3O_4/CeO_2 hybrid NWAs exhibit excellent pseudocapacitive performance with capacitance of 4.98 $F\cdot cm^{-2}$ at 10 $mA\cdot cm^{-2}$ (1037.5 $F\cdot g^{-1}$ at 2.08 $A\cdot g^{-1}$) and only a small capacitance loss of 5.6% after 5000 charge/discharge cycles. The remarkable pseudocapacitance and superior stability suggest that the mesoporous Co_3O_4/CeO_2 hybrid NWAs are promising candidates for supercapacitor applications.

Introduction

Supercapacitors (SCs), also known as electrochemical capacitor, have attracted intensive research interest in the past decade due to their excellent performance such as high power density, long life span and fast recharge features.[1-3] As is known to all, the morphology, size and composition of the electrode materials play a significant role in the performances of SCs. Among various materials, RuO_2 shows excellent supercapacitive performance, but its high cost and toxic feature impede the commercial applications severely.[4] Therefore, various metal oxides with low cost and benign environmental compatibility such as NiO, Co_3O_4, MnO_2 and so on have been employed as the electrode materials for SCs and investigated extensively to substitute RuO_2.[5-8] Especially, CeO_2, a rare earth metal oxide with good redox feature, environmentally benign nature and low cost, has intrigued the research interest in the application of supercapacitors in the past five years.[9-11] However, only part of surface electroactive materials can be effectively utilized to store charge due to the intrinsic poor electrical conductivity of single phase metal oxides, resulting in unsatisfactory SCs. Since T. Y. Wei and his colleagues[12] firstly constructed SCs based on $NiCo_2O_4$ with different morphologies, different kinds of $NiCo_2O_4$ nanostructures, such as nanoneedle arrays,[13] nanosheets,[14] nanowire[15] and nanorod arrays, [16] have been fabricated and used for the construction of SCs due to their good electrical conductivity, exhibiting excellent supercapacitive performance. In addition, element S was used to replace element O to fabricate $NiCo_2S_4$ nanostructures to further seek supercapacitive materials with improved performances. [17-19]

Recently, binary hybrid nanostructures with improved supercapacitive performance have received considerable attention.[20-23] Fan's research group constructed a novel Co_3O_4 nanowire@MnO_2 ultrathin nanosheet core/shell arrays for SCs, a capacitance of 480 $F\cdot g^{-1}$ was achieved at the current density of 2.67 $A\cdot g^{-1}$. [20] Subsequently, porous CoO@NiHON core/shell arrays were synthesized by the same research group, [21] this novel core/shell arrays exhibited specific capacitance of 798.3 $F\cdot g^{-1}$ at the current density of 1.67 $A\cdot g^{-1}$, meanwhile, both of these novel electrodes presented excellent long cycle stability. In general, it takes two procedures to fabricate core/shell arrays-based electrode for supercapacitors, which is time consuming and costly.

Therefore, it is attractive to get hybrid nanostructure arrays with high supercapacitive performance with a simple process. In this work, we report the synthesis of mesoporous Co_3O_4/CeO_2 hybrid NWAs with hydrothermal method. Impressively, as-prepared mesoporous Co_3O_4/CeO_2 hybrid NWAs exhibit remarkable pseudocapacitive performance with capacitance of 4.98 $F\cdot cm^{-2}$ at 10 $mA\cdot cm^{-2}$ (1037.5 $F\cdot g^{-1}$ at 2.08 $A\cdot g^{-1}$), which is much higher than that of Co_3O_4 nanowire arrays (1.95 $F\cdot cm^{-2}$ at 10 $mA\cdot cm^{-2}$ (670 $F\cdot g^{-1}$ at 3.33 $A\cdot g^{-1}$)). In addition, Co_3O_4/CeO_2 hybrid NWAs still present mesoporous structure after 5000 cycles and the capacitance loss is only 5.6%, showing excellent cycling stability.

Experimental

Synthesis of mesoporous Co_3O_4/CeO_2 hybrid NWAs

Mesoporous Co_3O_4/CeO_2 hybrid NWAs were synthesized by a hydrothermal process and calcinations process. In a typical synthesis, $Ce(NO_3)_3\cdot 6H_2O$ with different weight, 1.019 g $Co(NO_3)_3\cdot 6H_2O$ and 1.051 g urea were dissolved in 35 mL Milli-Q water. The mixture solution was transferred into a 50 ml Teflon-line stainless steel autoclave. Nickel foam (~2.5 cm×3 cm) rinsed with ethanol and 3 M HCl was immersed into the aforementioned mixture solution. Subsequently, the autoclave was kept in a conventional oven for 10 h at different temperatures and the autoclave was cooled down to room temperature naturally. As-prepared pink precursor (as shown in Fig. S1b, ESI†) was rinsed with Milli-Q water and ethanol several times and dried

under 80℃ for 24 h. Finally, the pink precursor was calcinated at 350℃ for 2 h and black products (as shown in Fig. S1c, ESI†) were obtained. Meanwhile, Co_3O_4 nanowire arrays were also fabricated by the same hydrothermal process with cobalt nitrate and urea to be taken as the control experiment. The influence of concentration of cerium nitrate in the mixture solution and hydrothermal temperature on the morphology and composition of Co_3O_4/CeO_2 hybrid NWAs was investigated and discussed. The loading masses of Co_3O_4 nanowires and Co_3O_4/CeO_2 hybrid nanowires were about 3.0 mg·cm^{-2} and 4.8 mg·cm^{-2}, respectively.

Materials characterization

The morphologies and composition of the samples were characterized by field emission scanning electron microscopy (FESEM, SU8020, Hitachi, Japan), transmission electron microscopy (TEM, JEM-2100F, JEOL, Japan) and energy dispersive spectrometer (EDS, Inca, Oxford, UK). The structures of the samples were measured by X-ray diffraction (XRD, D/MAX2500V, Rigaku, Japan) with Cu-K_α radiation (0.15418 nm) operating at 40 kV, 40 mA. Elemental status of the samples was analyzed by X-ray photoelectron spectrum (XPS, ESCALAB250, Thermo, US) with a monochromatic Al K_α (1486.6 eV) X-ray source.

Electrochemical measurements

The electrochemical measurements were carried out on an electrochemical workstation (Autolab PGSTAT302N, Metrohm, Switzerland) in a conventional three-electrode system in 2 M KOH aqueous solution at room temperature. Ni foam supported active materials (~1 cm^2 in area) was employed as the working electrode. Pt/Ti electrode and Ag/AgCl (3 M KCl) were used as counter electrode and reference electrode, respectively.

Electrochemical impedance spectrum (EIS) measurements were performed in a frequency range from 100 KHz to 0.1 Hz at an open circuit potential. The areal capacitance and specific capacitance were calculated according to the following equations:

$$C_s = I\Delta t/(S\Delta V) \quad (1)$$

$$C_{sp} = I\Delta t/(M\Delta V) \quad (2)$$

Where C_s (F·cm^{-2}) and C_{sp} (F·g^{-1}) represented areal capacitance and specific capacitance. I (A), Δt (s), S (cm^2), M (g) and ΔV (V) were discharge current, discharge time, area of the working electrode, the mass of active materials and the potential window excluding the IR drop.

Results and discussion

Synthesis and characterization of mesoporous Co_3O_4/CeO_2 hybrid NWAs

Fig. 1(a) and (b) show the SEM images of as-prepared samples after calcinations at 350 ℃ for 2 h. Apparently, nanowire arrays grow densely and vertically to the surface of the Ni foam and the average diameter of the nanowire is about 100 nm. In addition, the surface of nanowires is rather rough according to the observation in Fig. 1(b), and this is further confirmed by TEM observation and discussed in the following section. XRD patterns of the samples before and after calcinations are presented in Fig. 1 (c), XRD pattern of the sample before calcinations exhibits diffraction peaks of $CeCO_3OH$ (JCPDS 41-0013) and $Co(CO_3)_{0.5}(OH)\cdot 0.11H_2O$ (JCPDS 48-0083), and diffraction peaks in Fig. 1(b) curve A can be attributed to CeO_2 phase (JCPDS 34-0394) and Co_3O_4 phase (JCPDS 42-1467), indicating crystalline nature of Co_3O_4/CeO_2 hybrid NWAs after calcinations. The microstructural characterization of an individual Co_3O_4/CeO_2

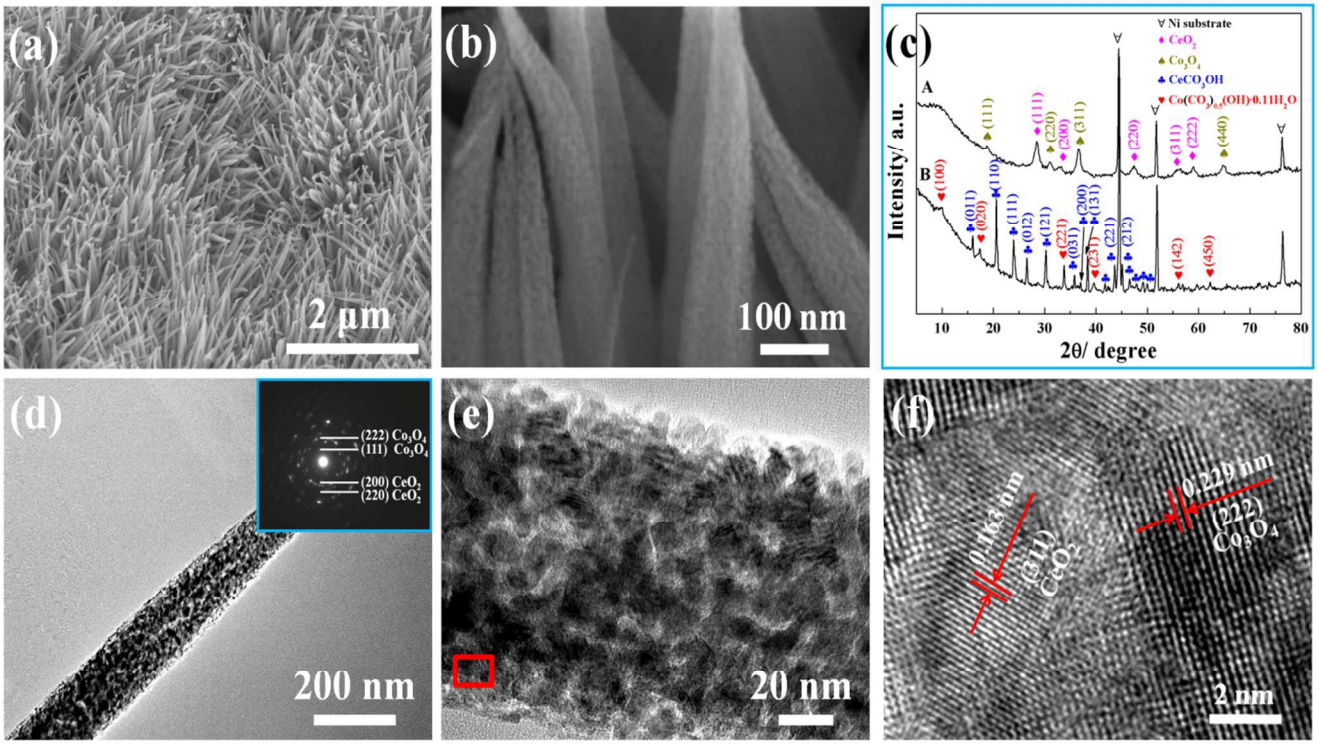

Fig. 1. SEM images of Co_3O_4/CeO_2 hybrid NWAs with (a) low and (b) high magnifications. (c) XRD pattern of as-prepared samples before and after calcinations. (d) and (e) are TEM images of an individual Co_3O_4/CeO_2 hybrid nanowire with different magnification, Inset in Fig. 1(d) is SAED pattern of the corresponding Co_3O_4/CeO_2 hybrid nanowire. (f) HRTEM image of Co_3O_4/CeO_2 hybrid nanowire.

hybrid nanowire is carried out in detail by TEM and HRTEM observation as shown in Figs. 1(d)-(f). Co_3O_4/CeO_2 hybrid nanowire exhibits porous structure and the pore size in the Co_3O_4/CeO_2 hybrid nanowire is between 2 and 10 nm. The mesoporous structure is further confirmed by the desorption data using the Barret-Joyner-Halenda (BJH) model as shown in Fig. S2 (a) and (b) (ESI †). BET surface area of as-prepared Co_3O_4/CeO_2 hybrid NWAs is calculated to be 88.15 $m^2 \cdot g^{-1}$. The mesoporous structure of Co_3O_4/CeO_2 hybrid NWAs is totally different from the smooth texture of their corresponding precursor as presented in Fig. S3 (ESI†), favouring the mass transport in the electrochemical reactions. Fig. 1(f) shows HRTEM image of an individual Co_3O_4/CeO_2 hybrid nanowire, the lattice fringes with lattice spacing of about 0.163 nm and 0.229 nm correspond to the (311) plane of CeO_2 and (222) plane of Co_3O_4, indicating the co-existence of CeO_2 phase and Co_3O_4 phase.

The chemical bonding states of samples are further investigated by XPS analysis as seen in Fig. 2. Fig. 2(a) shows Ce species is evidently detected in the Co_3O_4/CeO_2 hybrid NWAs. The O 1s spectrum in Fig. 2(b) exhibits three peaks centered at 529.4 eV, 530.3 eV and 530.9 eV, respectively. The two peaks centered at 529.4 eV and 530.9 eV are consistent with oxygen species in Co_3O_4 and adsorbed OH^- species on the surface of the samples. [24] Interestingly, the oxygen peak at 530.3 eV is ascribed to the oxygen bonded to cerium in CeO_2. In addition, the oxidation states of Co and Ce are determined by Co 2p and Ce 3d XPS spectra. As shown in Fig. 2(c), the Co 2p spectrum presents two main Co $2p_{3/2}$ and Co $2p_{1/2}$ peaks at 779.2 eV and 794.3 eV together with two shake-up satellite peaks, which are fitted with the chemical bonding states of Co_3O_4.[25, 26] Fig. 2(d) depicts the Ce 3d spectrum. The peaks centered at 881.6 eV, 888.5 eV, and 898.5 eV belong to Ce $3d_{5/2}$, and peaks at 900.7 eV, 903.6 eV, 907.2 eV and 916.4 eV correspond to Ce $3d_{3/2}$. Only the peak centered at 903.6 eV belongs to Ce^{3+}, and the other peaks are ascribed to Ce^{4+}.[27-29] XPS analysis is in agreement with the XRD pattern and HRTEM results shown in Fig. 1.

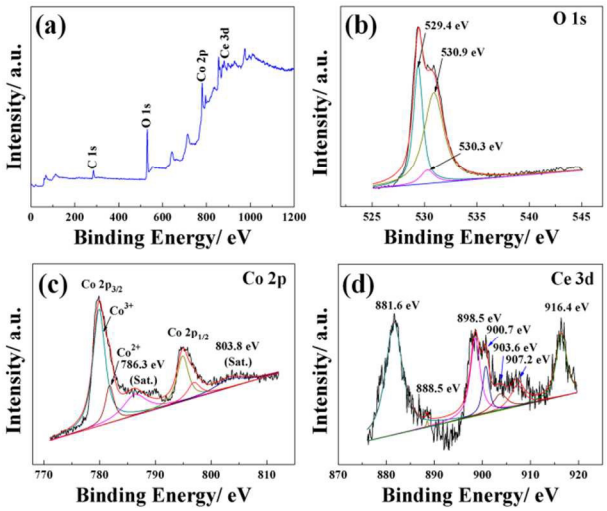

Fig. 2. (a) XPS survey spectra of Co_3O_4/CeO_2 hybrid NWAs, (b) O 1s, (c) Co 2p and (d) Ce 3d spectra of Co_3O_4/CeO_2 hybrid NWAs.

Energy dispersive X-ray spectroscopy (EDX) elemental mapping technique is employed to scrutinize compositional distribution of the hybrid nanowires. As shown in Fig. 3, Co, Ce and O elements distribute uniformly in an individual hybrid nanowire and the amount of Ce is less than that of Co, which is in agreement with the EDS analysis result (As shown in Fig. S4, ESI†). EDS result reveals the amount of Co and Ce is 48.0 wt.% and 3.5 wt.%, respectively. Interestingly, Co and Ce cannot form single phase compound like $NiCo_2O_4$ [15, 16, 30] or $MnCo_2O_4$ [31] in one-pot hydrothermal synthesis probably due to the significant chemical property differences between elements Ce and Co. In addition, the influences of cerium nitrate concentration and hydrothermal temperatures on the morphology, microstructure and composition of Co_3O_4/CeO_2 hybrid NWAs are also investigated systematically as shown in Fig. S5-S7, (ESI†). It is clearly observed in Fig. S5 that the morphology of Co_3O_4/CeO_2 hybrid NWAs is prone to be irregular if cerium nitrate concentration is beyond 100 mM and Co_3O_4/CeO_2 hybrid NWAs break and collapse when cerium nitrate concentration is more

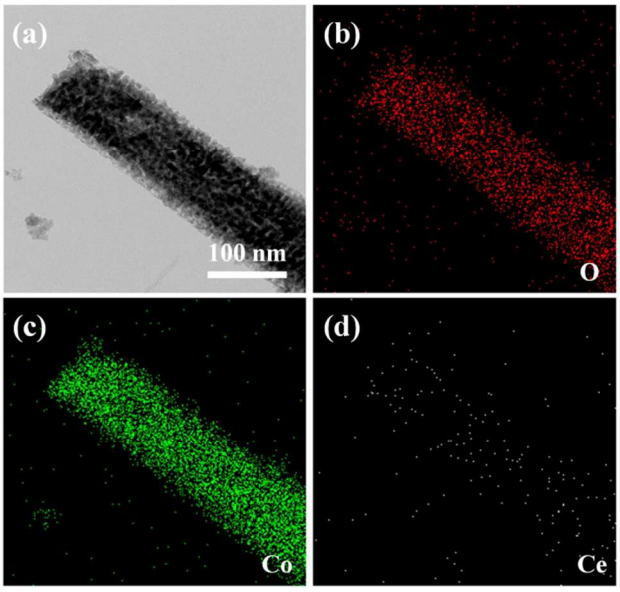

Fig. 3. (b-d) EDX mapping of (a) an individual Co_3O_4/CeO_2 hybrid nanowire.

than 200 mM. The hydrothermal temperature also plays a key role in controlling morphology, microstructure and composition of Co_3O_4/CeO_2 hybrid NWAs. Experimental results indicate that Co_3O_4/CeO_2 hybrid NWAs cannot be formed with hydrothermal temperature at 90 ℃. As shown in Fig. S6 (a) microballs with rough surface and different size are obtained. The phase structure of the microballs is characterized by X-ray diffraction analysis in Fig. S7, and as-obtained microballs can be determined as CeO_2 (JCPDS 34-0394) after calcinations at 350 ℃ for 2 h, which

reflects temperature is a key factor in the fabrication of Co_3O_4/CeO_2 hybrid NWAs. In addition, dependence of the hybrid nanowire composition on temperature is also investigated. Ce amounts in the hybrid nanowires prepared at 100 ℃, 110 ℃ and 120 ℃ are 1.8 wt%, 2.4 wt% and 3.5 wt%, respectively. In order to further investigate the composition of Co_3O_4/CeO_2 hybrid NWAs, Co/Ce molar ratios of Co_3O_4/CeO_2 hybrid NWAs are also measured by EDS equipped on TEM. Co/Ce molar ratios in Co_3O_4/CeO_2 hybrid NWAs decrease with the increase of hydrothermal temperature, they are measured to be 83.2, 43.9 and 26.3 at 100 ℃, 110 ℃ and 120 ℃, respectively.

To compare the difference between Co_3O_4/CeO_2 hybrid NWAs and Co_3O_4 NWAs, a control experiment is carried out by preparing phase-pure mesoporous Co_3O_4 NWAs following the same experimental procedure as growing the hybrid nanowire arrays. The electrochemical properties of the phase-pure mesoporous Co_3O_4 NWAs are determined as well. Morphology and microstructure information of Co_3O_4 NWAs are presented in Fig. S8 (ESI†), revealing that the Co_3O_4 NWAs has similar morphology to that of Co_3O_4/CeO_2 hybrid NWAs.

The main chemical reactions involved in the hydrothermal process and calcinations can be described as follows:[32]

$$CO(NH_2)_2 + H_2O \rightarrow 2NH_3 + CO_2 \quad (3)$$

$$CO_2 + H_2O \rightarrow CO_3^{2-} + 2H^+ \quad (4)$$

$$NH_3 \cdot H_2O \rightarrow NH_4^+ + OH^- \quad (5)$$

$$Co^{2+} + 0.5CO_3^{2-} + OH^- + 0.11\ H_2O \rightarrow Co(CO_3)_{0.5}(OH)\cdot 0.11H_2O \quad (6)$$

$$Ce^{3+} + CO_3^{2-} + OH^- \rightarrow CeCO_3OH \quad (7)$$

$$3Co(CO_3)_{0.5}(OH)\cdot 0.11H_2O + 0.5O_2 \rightarrow Co_3O_4 + 1.5CO_2 + 1.83H_2O \quad (8)$$

$$CeCO_3OH + 0.5O_2 \rightarrow CeO_2 + CO_2 + 0.5H_2O \quad (9)$$

Based on aforementioned results, the formation process of the mesoporous Co_3O_4/CeO_2 hybrid NWAs can be proposed here. Firstly, the $Co(CO_3)_{0.5}(OH)\cdot 0.11H_2O/CeCO_3OH$ hybrid NWAs precursors with smooth texture and compact structure are synthesized in the hydrothermal process, which is observed evidently in Fig. S3 (ESI†). Secondly, those precursors are converted to mesoporous Co_3O_4/CeO_2 hybrid NWAs *via in situ* decomposition and phase transformation in the calcinations process. During the calcinations process, $Co(CO_3)_{0.5}(OH)\cdot 0.11H_2O$ and $CeCO_3OH$ are converted Co_3O_4 and CeO_2 nanoparticles, respectively. The nucleation of the nanoparticles is random, but the growth of the nanoparticles is self-organized, retaining the shape of the nanowires. The weight loss and volume shrinking due to the release of gases such as CO_2 and H_2O in the calcinations process result in the mesoporous feature of Co_3O_4/CeO_2 hybrid NWAs, which is similar to the possibilities of the formation of mesoporous phase-pure Co_3O_4 NWAs reported previously. [33,34]

Electrochemical analysis

The cyclic voltammograms of CeO_2 NWAs, Co_3O_4 NWAs and Co_3O_4/CeO_2 hybrid NWAs are measured at a scan rate of 5 mV/s under the same condition as shown in Fig. 4(A). For CeO_2 NWAs and Co_3O_4 NWAs, the redox peaks are ascribed to the conversion between different cobalt and cerium oxidation states, the chemical reactions can be described as follows: [10, 29, 35]

$$CeO_2 + e^- + H_2O \leftrightarrow CeOOH + OH^- \quad (10)$$

$$Co_3O_4 + OH^- + H_2O \leftrightarrow 3CoOOH + e^- \quad (11)$$

$$CoOOH + OH^- \leftrightarrow CoO_2 + H_2O + e^- \quad (12)$$

Among these nanomaterials, the CV curve of CeO_2 NWAs (Fig. S9, ESI†) in Fig. 4(A) shows a much smaller enclosed area than those of Co_3O_4 NWAs and Co_3O_4/CeO_2 hybrid NWAs. The supercapacitive performances of Co_3O_4 NWAs and Co_3O_4/CeO_2 hybrid NWAs are further evaluated and compared by DC, EIS

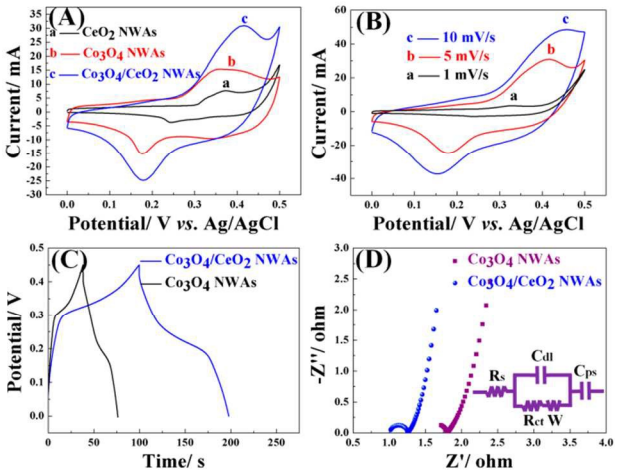

Fig. 4. (A) Cyclic voltammograms of different nanowire arrays at scan rate of 5 mV/s. (B) Cyclic voltammograms of Co_3O_4/CeO_2 NWAs at different scan rates. (C) Charge/discharge plots of Co_3O_4 and Co_3O_4/CeO_2 NWAs at the current density of 20 mA·cm^{-2}, and (D) Nyquist plots of Co_3O_4 and Co_3O_4/CeO_2 NWAs after fitting in 2 M KOH solution.

and cycling stability in the following section. Fig. 4(B) shows the CV curves of Co_3O_4/CeO_2 hybrid NWAs at different scan rates, the cathodic and anodic current peaks shift to both sides and increase with increasing scan rate. However, the capacitances of Co_3O_4/CeO_2 hybrid NWAs calculated from the enclosed areas of the CV curves are not changed significantly, suggesting a good rate capability. The galvanostatic charge/discharge (DC) measurements are performed to evaluate the supercapacitive performance of as-prepared samples. Fig. 4(C) presents the DC plots of Co_3O_4 NWAs and Co_3O_4/CeO_2 hybrid NWAs at the current density of 20 mA·cm^{-2}, the areal capacitance of Co_3O_4/CeO_2 hybrid NWAs is 4.68 F·cm^{-2}, much higher than that of Co_3O_4 NWAs (1.88 F·cm^{-2}). This is may be ascribed to the synergistic effect of Co_3O_4 and CeO_2. On the one hand, CeO_2 nanomaterials exhibit more surface defects due to their non-stoichiometric feature at ambient atmosphere. [36] The introduction of CeO_2 in Co_3O_4 NWAs further increases the surface defects of Co_3O_4/CeO_2 hybrid NWAs owing to the lattice mismatch between Co_3O_4 and CeO_2, resulting in a great improvement in surface redox properties of Co_3O_4/CeO_2 hybrid NWAs; on the other hand, Co_3O_4/CeO_2 hybrid NWAs demonstrate lower intrinsic resistance compared to phase-pure Co_3O_4 NWAs, reducing charge transfer resistance and leading to fast electron transport within active materials. And this is confirmed by electrochemical impedance spectra (EIS) as seen in Fig. 4(D). Fig. 4(D) shows the Nyquist plots after fitting with equivalent electrical circuit, which contains solution resistance R_s, charge transfer resistance R_{ct}, Warburg impedance, double layer capacitance C_{dl} and pseudocapacitance C_{ps} as shown in inset in Fig. 4(D).[37,38] In the low frequency portion, the slope of the curve

reveals the Warburg impedance, reflecting the electrolyte diffusion in the mesoporous electrode. The slope of Co_3O_4/CeO_2 hybrid NWAs is almost the same as that of Co_3O_4 NWAs in Fig. 4(D), which means electrolyte diffusion at electrolyte/(Co_3O_4/CeO_2 hybrid NWAs) interfaces is similar to that between electrolyte and Co_3O_4 NWAs. In the high frequency portion, charge transfer resistance R_{ct} shows the charge transfer process between electrolyte and Co_3O_4/CeO_2 (Co_3O_4) NWAs. According to the fitted data, Co_3O_4/CeO_2 hybrid NWAs (0.243 Ω) demonstrate lower charge transfer resistance R_{ct} than that of Co_3O_4 NWAs (0.274 Ω). It is believed that a lower charge transfer resistance R_{ct} can contribute to the improvement of supercapacitive performance of Co_3O_4/CeO_2 hybrid NWAs.

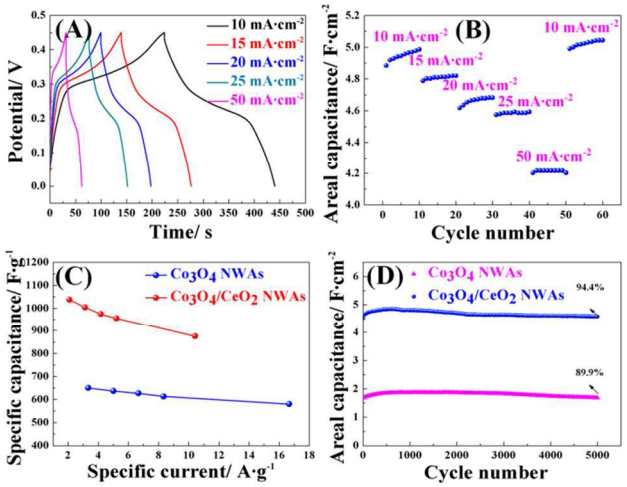

Fig. 5. (a) Charge/discharge plots and (b) corresponding areal capacitances of Co_3O_4/CeO_2 hybrid NWAs at different current densities. (c) Specific capacitances of Co_3O_4 NWAs and Co_3O_4/CeO_2 hybrid NWAs at different specific current. (d) Cycling performance of Co_3O_4 NWAs and Co_3O_4/CeO_2 hybrid NWAs at 20 mA·cm^{-2}.

Fig. 5(a) depicts the DC plots of Co_3O_4/CeO_2 hybrid NWAs in the potential window between 0 and 0.45 V (*vs.* Ag/AgCl). Co_3O_4/CeO_2 hybrid NWAs exhibit areal capacitances with 4.98 F·cm^{-2} at 10 mA·cm^{-2}, 4.82 F·cm^{-2} at 15 mA·cm^{-2}, 4.68 F·cm^{-2} at 20 mA·cm^{-2}, 4.59 F·cm^{-2} at 25 mA·cm^{-2} and and 4.2 F·cm^{-2} at 50 mA·cm^{-2}, respectively, as demonstrated in Fig. 5(a) and (b). In addition, the pseudocapacitance loss is only 15.7% when current density changes from 10 mA·cm^{-2} to 50 mA·cm^{-2} during charge/discharge process, and the areal capacitance recovers to ~4.98 F·cm^{-2} when current density turns back to 10 mA·cm^{-2}, indicating good rate capability of the Co_3O_4/CeO_2 hybrid NWAs. Meanwhile, supercapacitive performances of Co_3O_4 NWAs are also evaluated by charge/discharge measurements under the same condition as Co_3O_4/CeO_2 hybrid NWAs as demonstrated in Fig. S10-S11 (ESI†). Areal capacitances of the Co_3O_4 NWAs are measured to be 1.95 F·cm^{-2} at 10 mA·cm^{-2}, 1.91 F·cm^{-2} at 15 mA·cm^{-2}, 1.88 F·cm^{-2} at 20 mA·cm^{-2}, 1.84 F·cm^{-2} at 25 mA·cm^{-2} and and 1.74 F·cm^{-2} at 50 mA·cm^{-2}, respectively. It can be seen that the capacitance of the Co_3O_4 NWAs is much lower than that of Co_3O_4/CeO_2 hybrid NWAs due to aforementioned reasons. Fig. 5(c) shows the specific capacitances of both Co_3O_4 NWAs and Co_3O_4/CeO_2 hybrid NWAs at different current densities, which are calculated according to the areal capacitances and loading mass of active materials. As for Co_3O_4 NWAs, the specific capacitance achieves 650 F·g^{-1} (1.95 F·cm^{-2}) at 3.33 A·g^{-1} (10 mA·cm^{-2}) and 613.3 F·g^{-1} (1.84 F·cm^{-2}) at 8.33 A·g^{-1} (25 mA·cm^{-2}), which are much lower than those hybrid nanowires of 1037.5 F·g^{-1} (4.98 F·cm^{-2}) at 2.08 A·g^{-1} (10 mA·cm^{-2}) and 875.0 F·g^{-1} (4.2 F·cm^{-2}) at 10.4 A·g^{-1}(50 mA·cm^{-2}) due to synergistic effect of Co_3O_4 and CeO_2 discussed aforementioned. In addition, the capacitances of this novel Co_3O_4/CeO_2 hybrid NWAs are higher than those previously reported Co_3O_4-based hybrid materials, such as Co_3O_4/MnO_2 core/shell hybrid arrays (480.0 F·g^{-1} at 2.67 A·g^{-1}),[20] Co_3O_4@PPy@MnO_2 hybrid NWAs (629.0 F·g^{-1} at 0.67 A·g^{-1}),[39] Co_3O_4/NiO hybrid NWAs (853.0 F·g^{-1} at 2.0 A·g^{-1}),[40] Co_3O_4@Ag hybrid NWAs (1006.0 F·g^{-1} at 2.0 A·g^{-1}).[41] Performances of supercapacitors based on different Co_3O_4-based NWAs are compared and summarized in Table S1(ESI †). Evidently, the synthesis of Co_3O_4/CeO_2 hybrid NWAs with one-step hydrothermal method is facile and cost effective compared to multiple procedures for the fabrication of other Co_3O_4-based NWAs, and high mass loading of Co_3O_4/CeO_2 hybrid NWAs favours the improvement of rate capability of supercapacitors.[42]

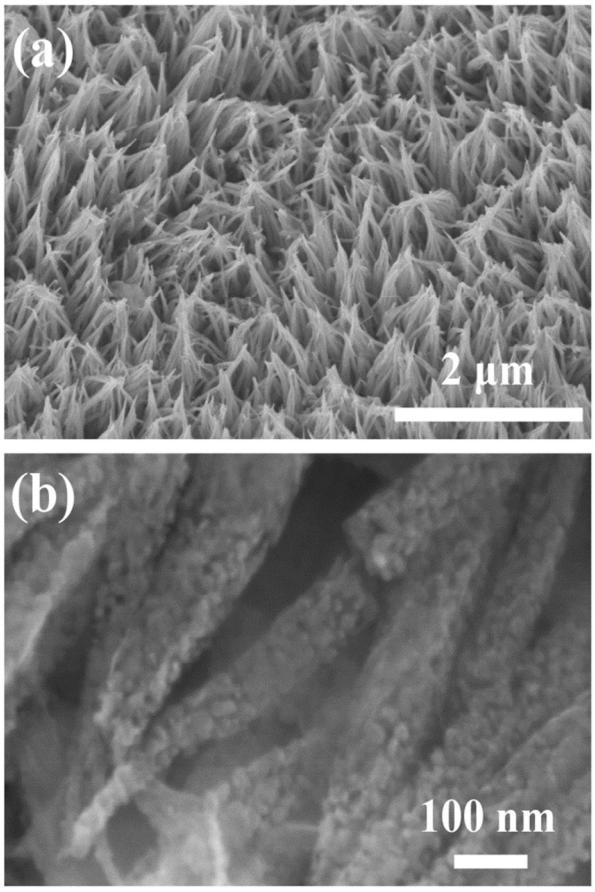

Fig. 6 SEM images of Co_3O_4/CeO_2 hybrid NWAs after cycling for 5000 cycles with low (a) and high (b) magnifications.

The cycling stabilities of both Co_3O_4 NWAs and Co_3O_4/CeO_2 hybrid NWAs are evaluated at the current density of 20 mA·cm^{-2} as shown in Fig. 5(d). The results show that 94.4% and 89.9% capacitances of the products are remained after 5000 cycles for Co_3O_4/CeO_2 hybrid NWAs and Co_3O_4 NWAs, respectively. The

enhanced electrochemical cycling performance of the Co_3O_4/CeO_2 hybrid NWAs can be attributed to the synergistic effect of Co_3O_4 and CeO_2, which not only increases the capacitance but also improves the stability. On the one hand, faradic redox reaction of Ce^{3+}/Ce^{4+} further increases the capacitance of the Co_3O_4/CeO_2 hybrid NWAs compared to phase-pure Co_3O_4 NWAs,[10] on the other hand, reduced charge transfer resistance R_{ct} also favours the capacitance improvement of Co_3O_4/CeO_2 hybrid NWAs. In addition, the incorporation of CeO_2 in the Co_3O_4/CeO_2 hybrid NWAs improves the cycling stability due to the superior chemical stability of CeO_2, and this is further confirmed by the SEM characterization of Co_3O_4/CeO_2 hybrid NWAs after 5000 cycles as observed in Fig. 6. Figs. 6 (a) and (b) show SEM images of Co_3O_4/CeO_2 hybrid NWAs after 5000 cycles with different magnifications. The images reveal that the morphology of Co_3O_4/CeO_2 hybrid NWAs after 5000 cycles is well-preserved. In addition, the crystallinity and mesoporous structure of Co_3O_4/CeO_2 nanowire remains undamaged as well in the charge/discharge process with long time. The BET surface area (83.46 $m^2 \cdot g^{-1}$) decreases and the pore size increases slightly of Co_3O_4/CeO_2 hybrid NWAs after 5000 cycles, which can also be evidenced in Fig. S2 (c).

Conclusions

In summary, we have developed a facile and effective approach for the fabrication mesoporous Co_3O_4/CeO_2 hybrid NWAs on Ni foam. This novel hybrid nanostructure combines the merits of two active materials (Co_3O_4 and CeO_2) and exhibits excellent pseudocapacitive performances. Mesoporous Co_3O_4/CeO_2 hybrid NWAs are superior to Co_3O_4 NWAs in terms of specific capacitance and cycling stability. The cost-effective synthesis and remarkable supercapacitive performance makes this novel hybrid an excellent active material in the applications of supercapacitors.

Acknowledgements

The authors acknowledge the financial supports of National Natural Science Foundation of China (Grant Nos. 51302060 and 51402081), financial supports of the National Key Fundamental Research Development Program (Grant No. 2014CB660815). Financial supports of Natural Science Foundation of Anhui Province (Grant No. 1408085QB42) and Scientific and Technological Project of Anhui Province (1301b042011) are also gratefully appreciated. J. W. Cui thanks the staff in the Analytical and Testing Center of HFUT for their assistance in the materials characterization.

Notes and references

[a] *School of Materials Science and Engineering, Hefei University of Technology, Hefei,230009, China; E-mail:ycwu@hfut.edu.cn*
[b] *Key Laboratory of Advanced Functional Materials and Devices of Anhui Province, Hefei, 230009, China*
[c] *School of Chemistry, Monash University, Clayton, VIC 3800, Australia*

† Electronic Supplementary Information (ESI †) available: [Optical photograph of as prepared samples, SEM, TEM, EDS, XRD, EDX mapping of the samples are presented. DC plots and corresponding areal capacitances of Co_3O_4 NWAs at different current densities are shown here]. See DOI: 10.1039/b000000x/

1 P. Simon and Y. Gogotsi, Nat. Mater., 2008, 7, 845-854.
2 J. R. Miller and P. Simon, Science, 2008, 321, 651-652.
3 G. Wang, L. Zhang and J. Zhang, Chem. Soc. Rev., 2012, 41, 797-828.
4 C. C. Hu, K. H. Chang, M. C. Lin and Y. T. Wu, Nano Lett. 2006, 6, 2690-2695.
5 N. S. Liu, J. Li, W. Z. Ma, W. J. Liu, Y. L. Shi, J. Y. Tao, X. H. Zhang, J. Su, L. Y. Li and Y. H. Gao, ACS Appl. Mater. Interfaces, 2014, 6,13627-13634.
6 X. H. Xia, J. P. Tu, Y. J. Mai, X. L.Wang, C. D. Gu and X. B. Zhao, J. Mater. Chem., 2011, 21, 9319-9325.
7 Y. Z. Zhang, Y. Wang, Y. L. Xie, T. Cheng, W. Y. Lai, H. Pang and W. Huang, Nanoscale, 2014, 6, 14354-14359.
8 Z. B. Lei, F. H Shi and L. Lu, ACS Appl. Mater. Interfaces, 2012, 4, 1058-1064.
9 Y. Wang, C. X. Guo, J. H. Liu, T. Chen, H. B. Yang and C. M. Li, Dalton Trans., 2011, 40, 6388-6391.
10 N. Padmanathan and S. Selladurai, RSC Adv., 2014, 4, 6527-6534.
11 S. Maiti, A. Pramanik and S. Mahanty, Chem. Commun., 2014, 50, 11717-11720.
12 T. Y. Wei, C. H. Chen, H. C. Chien, S. Y. Lu and C. C. Hu, Adv. Mater., 2010, 22, 347-351.
13 G. Q. Zhang, H. B.Wu , H. E.Hoster, M. B. Chan-Park and X. W. Lou, Energy Environ. Sci., 2012, 5, 9453-9456.
14 G. Q. Zhang and X. W. Lou, Adv. Mater., 2013, 25, 976-979.
15 H. Jiang, J. Ma and C. Z. Li, Chem. Commun., 2012, 48, 4465-4467.
16 G. Q. Zhang and X. W. Lou, Sci. Rep. 2013, 3, 1470(1-6).
17 J. W. Xiao, L. Wan, S. H. Yang, F. Xiao and S. Wang. Nano Lett., 2014, 14,831-838.
18 M. Sun, J. Tie, G. Cheng, T. Lin, S. Peng, F. Deng, F. Ye and L. Yu, J. Mater. Chem. A, 2015, 3, 1730-1736..
19 L. F. Shen, J. Wang, G. Y. Xu, H.S. Li, H. Dou and X. G. Zhang, Adv. Energy Mater., 2014, DOI: 10.1002/AENM.201400977.
20 J. P. Liu, J. Jiang, C. W. Cheng, H. X. Li, J. X. Zhang, H. Gong and H. J. Fan, Adv. Mater., 2011, 23, 2076-2081.
21 C. Guan, J. P. Liu, C. W. Cheng, H. X. Li, X. L. Li, W. W. Zhou, H. Zhang and H. J. Fan, Energy Environ. Sci., 2011, 4, 4496-4499.
22 L. Yu, G. Q. Zhang, C. Z. Yuan and X. W. Lou, Chem. Commun., 2013, 49, 137-139.
23 J. Yang, M. Z. Ma, C. C. Sun, Y. F. Zhang, W. Huang and X. C. Dong, J. Mater. Chem. A, 2015, 3, 1258-1264.
24 D. W. Wang, Q. H. Wang and T. M. Wang, Inorg. Chem., 2011, 50,6482-6492.
25 Y. Tak and K. Yong, J. Phys. Chem. C, 2008, 112,74-79.
26 D. B. Yu, Y. L. Wang, L. Zhang, Z. X. Low, X. Y. Zhang, F. L. Chen, Y. Feng and H. T. Wang, Nano Energy, 2014, 10, 153-162.
27 F. F. Zhu, G. Z. Chen, S. X. Sun and Y. Sun, J. Mater. Chem. A, 2013, 1, 288-294.
28 T. Wang, L. D. Zhang, J. X. Zhang and G. M. Hua, Micropor. Mesopor. Mater., 2013, 171, 196-200.
29 C. Zhang, X. Y. Zhang, Y. C. Wang, S. L. Xie, Y. Liu, X. H. Lu and Y. X. Tong, New J. Chem., 2014, 38, 2581-2586.
30 C. Z. Yuan, J. Y. Li, L. R. Hou, X. G. Zhang, L. F. Shen and X. W. Lou, Adv. Funct. Mater., 2012, 22, 4592-4597.
31 A. K. Mondai, D. W. Su, S. Q. Chen, A. Ung, H. S. Kim and G. X. Wang, Chem.- Eur. J., 2015, 21, 1526-1532.
32 X. H. Xia, J. P. Tu, Y. Q. Zhang, Y. J. Mai, X. L. Wang, C. D. Gu and X. B. Zhao, RSC Adv., 2012, 2, 1835-1841.
33 G. X. Wang, X. P. Shen, J. Horvat, B. Wang, H. Liu, D. Wexler and J. Yao,J. Phys. Chem. C, 2009, 113, 4357-4361.
34 F. Zhang, C. Z. Yuan, X. J. Lu, L. J. Zhang, Q. Che and X. G. Zhang, J. Power Sources, 2012, 203, 250-256.
35 H. T. Wang, L. Zhang, X. H. Tan, C. M. B. Holt, B. Zahiri, B. C. Olsen and D. Mitlin, J. Phys. Chem. C, 2011, 115, 17599-17605.
36 D. S. Zhang, X. J. Du L. Y. Shi and R. H. Gao, Dalton Trans., 2012, 41, 14455-14475.
37 Q. W. Zhou, J. C. Xing, Y. F. Gao, X. J. Lv, Y. M. He, Z. H. Guo and Y. M. Li, ACS Appl. Mater. Interfaces 2014, 6, 11394-11402.
38 S. K. Meher and G. R. Rao, J. Phys. Chem. C, 2011, 115, 15646-15654.
39 L. J. Han, P. Y. Tang and L. Zhang, Nano Energy, 2014, 7, 42-51.

40 X. C. Dong, H. Xu, X. W. Wang,Y.X. Huang, M. B. Chan-Park, H. Zhang, L. H. Wang,W. Huang and P. Chen, ACS Nano, 2012, 6, 3206-3213.
41 H. Cheng, Z. G. Lu, J. Q. Deng, C. Y. Chung, K. L. Zhang and Y. Y. Li, Nano Res., 2010, 3, 895-901.
42 A. Sumboja, X. Wang, J. Yan and P. S. Lee, Electrochim. Acta, 2012, 65, 190-195.

Mesoporous Co_3O_4/CeO_2 hybrid nanowire arrays are synthesized and employed as the electrode materials for supercapacitors. This nanomaterials exhibit remarkable pseudocapacitance and superior cycling stability.